



## Article

# High Selectivity, Low Damage ICP Etching of *p*-GaN over AlGaN for Normally-off *p*-GaN HEMTs Application

Penghao Zhang <sup>1</sup>, Luyu Wang <sup>1</sup>, Kaiyue Zhu <sup>2</sup>, Yannan Yang <sup>1</sup>, Rong Fan <sup>1</sup>, Maolin Pan <sup>1</sup>, Saisheng Xu <sup>1</sup>, Min Xu <sup>1,\*</sup>, Chen Wang <sup>1,\*</sup>, Chunlei Wu <sup>1</sup> and David Wei Zhang <sup>1,\*</sup>

<sup>1</sup> State Key Laboratory of ASIC and System, School of Microelectronics, Fudan University, Shanghai 200433, China; phzhang19@fudan.edu.cn (P.Z.); wangly20@fudan.edu.cn (L.W.); yangyn20@fudan.edu.cn (Y.Y.); 20212020129@fudan.edu.cn (R.F.); 21112020100@m.fudan.edu.cn (M.P.); ssxu@fudan.edu.cn (S.X.); wuchunlei@fudan.edu.cn (C.W.)

<sup>2</sup> Department of Electrical and Electronic Engineering, Xi'an Jiaotong-Liverpool University, Suzhou 215123, China; kaiyue.zhu18@student.xjtlu.edu.cn

\* Correspondence: xu\_min@fudan.edu.cn (M.X.); chen\_w@fudan.edu.cn (C.W.); dwzhang@fudan.edu.cn (D.W.Z.)

**Abstract:** A systematic study of the selective etching of *p*-GaN over AlGaN was carried out using a BCl<sub>3</sub>/SF<sub>6</sub> inductively coupled plasma (ICP) process. Compared to similar chemistry, a record high etch selectivity of 41:1 with a *p*-GaN etch rate of 3.4 nm/min was realized by optimizing the SF<sub>6</sub> concentration, chamber pressure, ICP and bias power. The surface morphology after *p*-GaN etching was characterized by AFM for both selective and nonselective processes, showing the exposed AlGaN surface RMS values of 0.43 nm and 0.99 nm, respectively. MIS-capacitor devices fabricated on the AlGaN surface with ALD-Al<sub>2</sub>O<sub>3</sub> as the gate dielectric after *p*-GaN etch showed the significant benefit of BCl<sub>3</sub>/SF<sub>6</sub> selective etch process.

**Keywords:** *p*-GaN; selective etching; ICP; surface morphology; MIS capacitor



**Citation:** Zhang, P.; Wang, L.; Zhu, K.; Yang, Y.; Fan, R.; Pan, M.; Xu, S.; Xu, M.; Wang, C.; Wu, C.; et al. High Selectivity, Low Damage ICP Etching of *p*-GaN over AlGaN for Normally-off *p*-GaN HEMTs Application. *Micromachines* **2022**, *13*, 589. <https://doi.org/10.3390/mi13040589>

Academic Editor: Kun Li

Received: 8 March 2022

Accepted: 6 April 2022

Published: 9 April 2022

**Publisher's Note:** MDPI stays neutral with regard to jurisdictional claims in published maps and institutional affiliations.



**Copyright:** © 2022 by the authors. Licensee MDPI, Basel, Switzerland. This article is an open access article distributed under the terms and conditions of the Creative Commons Attribution (CC BY) license (<https://creativecommons.org/licenses/by/4.0/>).

## 1. Introduction

GaN-based high electron mobility transistors (HEMTs) have recently attracted much attention in applications for power switching due to their properties of high-frequency and low on-resistance [1,2]. Two-dimensional-electron-gas (2DEG) is induced by the strong spontaneous and piezoelectric polarization effect in the AlGaN/GaN heterojunction [3], which causes the conventional devices normally be on, i.e., depletion-mode. However, normally-off, i.e., enhanced-mode transistors with a positive threshold voltage are more desirable for simplified circuit design in practice [4,5]. To deplete the 2DEG under the gate area, several approaches have been invented, such as fluorine-implanted treatment [6], gate-recessed [7] and *p*-GaN gate structure [8]. Among these technologies, *p*-GaN gate HEMTs show broad market prospects [9,10].

Precise etch depth control of the *p*-GaN layer with minimum etch damage to the underlying AlGaN barrier is necessary to recover high-density electrons in the access regions, which is the most critical process in the fabrication of *p*-GaN gate HEMTs [11]. Generally, to fully deplete the 2DEG in the channel for normally off operation, a thick *p*-GaN layer with a thin AlGaN layer in epitaxy technique is employed. Further thinning of the AlGaN barrier due to overetching, even a few nanometers, could lead to a dramatic reduction in the conductivity in the access region, which means degradation of the output performance of the devices [12]. On the other hand, an underetched Mg-doped *p*-GaN layer could form a conducting channel contributing to off-state leakage [13]. Therefore, the precise control of *p*-GaN etch depth with minimum damage on AlGaN surface is needed for higher performance E-mode HEMT devices with higher drive current, lower off-leakage and improved dynamic on-resistance [14].

As reported in reference [15], adding SF<sub>6</sub> gas to BCl<sub>3</sub> gas would form an AlF<sub>x</sub> nonvolatile layer on the surface of AlGa<sub>0.25</sub>N layer after GaN removal, thus achieving high selectivity between GaN and AlGa<sub>0.25</sub>N, as of 23:1. However, the detailed process optimization and the corresponding impact on the etch damage of AlGa<sub>0.25</sub>N surface have not been studied yet. In this work, a highly selective ICP etching of *p*-GaN over AlGa<sub>0.25</sub>N by the BCl<sub>3</sub>/SF<sub>6</sub> mixture was systematically investigated. The influence of chamber pressure, SF<sub>6</sub> gas flow, ICP power and bias power on the etch rates and selectivity were studied. The highest selectivity was obtained through process optimization for BCl<sub>3</sub>/SF<sub>6</sub> etch ambient. Atomic force microscope (AFM) image of AlGa<sub>0.25</sub>N layer exposed after *p*-GaN selective etching showed a very smooth surface. C–V measurements for Ni/Al<sub>2</sub>O<sub>3</sub>/AlGa<sub>0.25</sub>N stack MIS structure further confirmed the advantage of this high selective etch process and the minimum etch damage on AlGa<sub>0.25</sub>N surface.

## 2. Experimental

In this work, two commercially available *p*-GaN/AlGa<sub>0.25</sub>N/GaN and AlGa<sub>0.25</sub>N/GaN hetero-structures epitaxially grown on 6-inch Si substrate were used. One is *p*-GaN (80 nm)/Al<sub>0.25</sub>Ga<sub>0.75</sub>N (15 nm)/unintentionally doped GaN (300 nm)/buffer (4.2 μm)/Si (1 mm), and the other is Al<sub>0.25</sub>Ga<sub>0.75</sub>N (15 nm)/unintentionally doped GaN (300 nm)/buffer (4.2 μm)/Si (1 mm). They are referred to *p*-GaN sample and AlGa<sub>0.25</sub>N sample in the rest of this article.

The etch chamber used to develop the selective *p*-GaN etch process is a customized ICP tool from NAURA (NAURA Technology Group Co., Ltd., Beijing, China) with designed bias power as low as 5 W. For all the processes, a pure BCl<sub>3</sub> plasma pre-etching was carried out to punch through the (Al)Ga<sub>0.25</sub>N native oxide on the exposed surface [16], right before the main BCl<sub>3</sub>/SF<sub>6</sub> etch.

The frequencies of power generator and chamber chiller temperature were set as 13.56 MHz and 20 °C, respectively. Etch process conditions were optimized with SF<sub>6</sub> concentration in the range of 0–30% (constant total flow of 150 sccm), chamber pressure in the range of 20–60 mTorr, ICP power in the range of 200–600 W and bias power in the range of 20–80 W. *p*-GaN and AlGa<sub>0.25</sub>N samples were etched simultaneously for process evaluation. The etch depth and surface morphology were evaluated using a Park NX10 AFM. Z scanner resolution of this AFM reached 0.015 nm in order that etch depth of patterned samples could be precisely characterized. Etching profiles were inspected by scanning electron microscopy (SEM), and selectivity was calculated as the ratio of the etch rate of *p*-GaN to AlGa<sub>0.25</sub>N.

## 3. Results and Discussion

### 3.1. Etching Parameter Optimization

#### 3.1.1. SF<sub>6</sub> Concentration

The selective etch process has a strong dependence on the SF<sub>6</sub> concentration in the ambient, as presented in Figure 1. The other etching conditions were fixed as follows: chamber pressure of 40 mTorr, ICP power of 600 W and bias power of 40 W. A significant enhancement in the *p*-GaN etch rate is observed when the SF<sub>6</sub> concentration increases from 0 to 15% due to the catalyzed generation of the active chlorine [17,18]. However, further increasing SF<sub>6</sub> gas flow leads to a decrease in the *p*-GaN etch rate due to the formation of involatile GaF<sub>x</sub> [18,19]. In summary, adding SF<sub>6</sub> has two-side impacts on the etch of *p*-GaN and the concentration could be optimized to have the best *p*-GaN etch. For the AlGa<sub>0.25</sub>N sample, the etch rate monotonically decreases with increasing SF<sub>6</sub> concentration due to the formation of nonvolatile AlF<sub>x</sub> acting as a powerful etch-stop layer [15]. The selectivity reaches a maximum at 15% SF<sub>6</sub>.

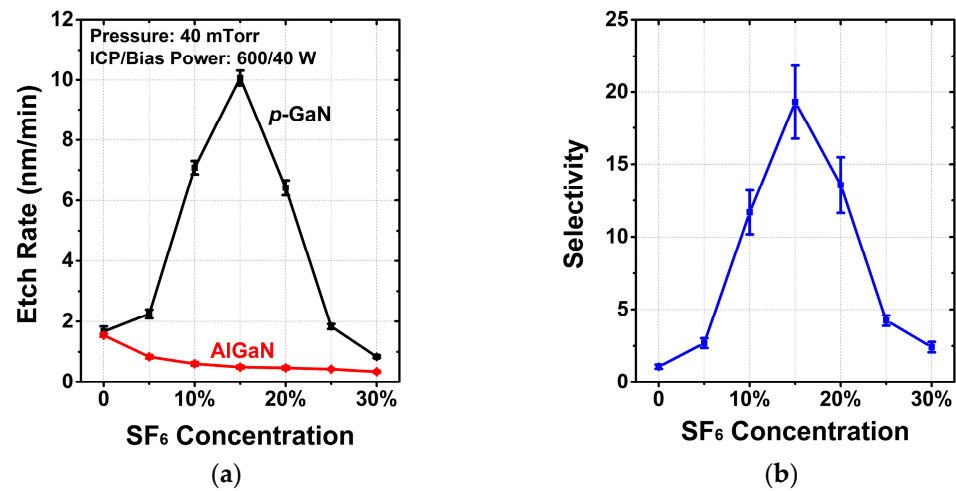


Figure 1. Dependence of (a) the etch rates, (b) selectivity between  $p\text{-GaN}$  and  $\text{AlGaIn}$  on  $\text{SF}_6$  concentration.

### 3.1.2. Chamber Pressure

The effects of chamber pressure on the etch rates of  $p\text{-GaN}$  and  $\text{AlGaIn}$  layers and the selectivity were examined, as shown in Figure 2. The other etching conditions were fixed as follows:  $\text{SF}_6$  concentration of 15%, ICP power of 600 W and bias power of 40 W. At the beginning of increasing chamber pressure, more chemical radicals of chlorine are generated to react with  $p\text{-GaN}$  in order that the etch rate keeps increasing. When the pressure is higher than 40 mTorr, the formed involatile  $\text{GaF}_x$  becomes the dominant to suppress the etching of  $p\text{-GaN}$ . For  $\text{AlGaIn}$ , more  $\text{AlF}_x$  will be formed with higher pressure to reduce the etch rate. The etch selectivity increases from 5:1 to 24:1 as the chamber pressure increases from 20 to 60 mTorr. However, there is a trade-off in the pressure range of 40–60 mTorr, considering the slight improvement in selectivity and the sharp drop of  $p\text{-GaN}$  etch rate.

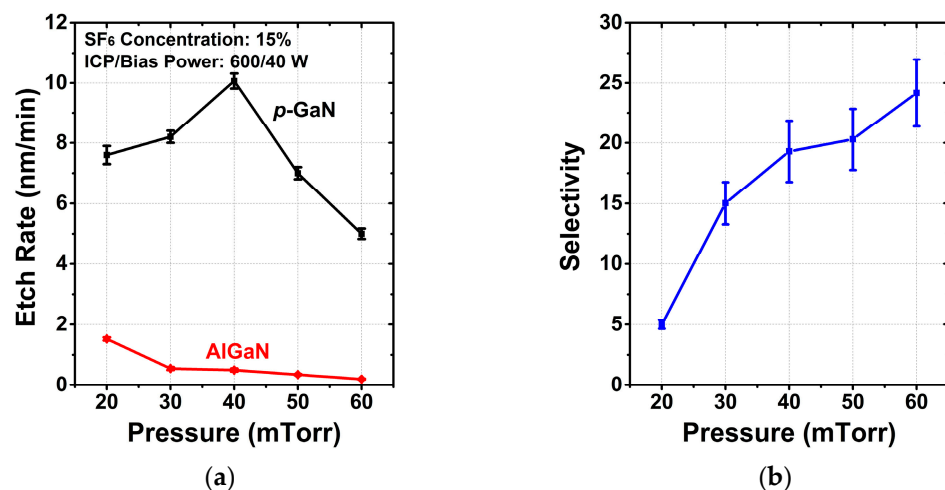


Figure 2. Dependence of (a) the etch rates, (b) selectivity between  $p\text{-GaN}$  and  $\text{AlGaIn}$  on chamber pressure.

### 3.1.3. ICP Power

The ICP etching mechanism is a combined process of chemical reaction and ion sputtering. Both plasma density and ion energy can be regulated independently with two RF generators, i.e., ICP and bias power generators. Thus, the variation of source power and bias power can effectively affect the proportion of chemical and physical etching.

The etch rates, selectivity and self-bias voltage as a function of ICP power are shown in Figure 3. The other etching conditions were fixed as follows:  $\text{SF}_6$  concentration of 15%, pressure of 40 mTorr and bias power of 40 W. The plasma density and fractional ionization

are controlled by the ICP power. The etch rate of the *p*-GaN sample remarkably increases from 1.3 to 10.1 nm/min with increasing ICP power from 200 to 600 W due to more activity and density of the chemical radicals. The declining self-bias voltage is associated with increasing plasma density, indicating that the plasma bombardment is weakened. Increasing chemical reaction proportion and decreasing physical bombardment are exactly desired for high selectivity and low etch damage. However, the AlGaIn etch rate slightly increases owing to the competition between chlorine as the etching agent and fluorine as the inhibition agent.  $\text{AlF}_x$  can be formed more easily than  $\text{GaF}_x$ , preventing a quick increase of AlGaIn etching. As a result, the *p*-GaN/AlGaIn etch selectivity increases with ICP power.

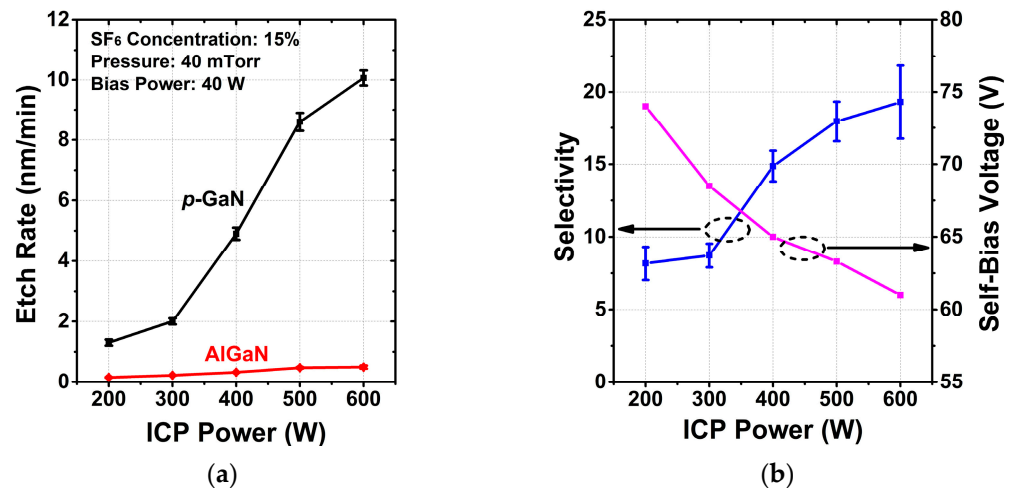


Figure 3. Dependence of (a) the etch rates, (b) selectivity between *p*-GaN and AlGaIn and self-bias voltage on ICP power.

#### 3.1.4. Bias Power

The effects of bias power are shown in Figure 4. The other etching conditions were fixed as follows:  $\text{SF}_6$  concentration of 15%, pressure of 40 mTorr and ICP power of 600 W. The bias power is strongly related to physical etching. The self-bias voltage decreases linearly as the bias power decreases, indicating reduced ion bombardment energy. Though both *p*-GaN and AlGaIn etch rates decrease proportionally to the decreasing bias power, almost linearly increasing selectivity is obtained. When the bias power drops down to 20 W, the selectivity reaches a maximum of 41:1 at a *p*-GaN etch rate of 3.4 nm/min in this study. The reduction in selectivity at high bias power can be explained in terms of enhanced sputtering of the  $\text{AlF}_x$  film at the AlGaIn surface.

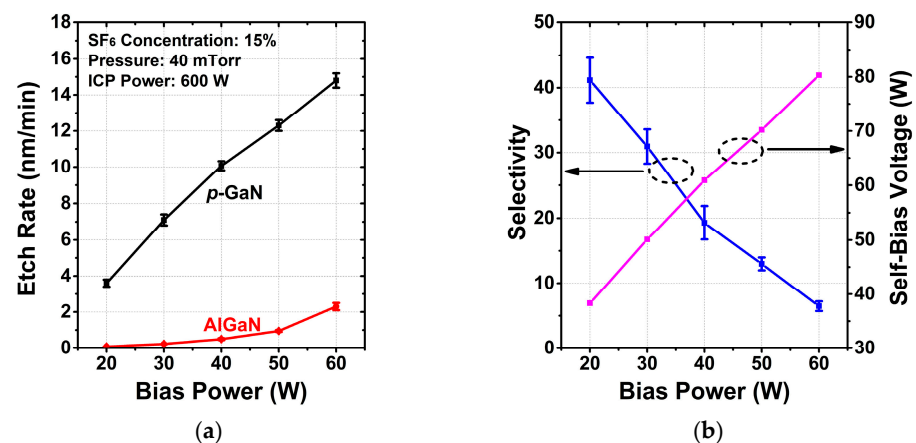


Figure 4. Dependence of (a) the etch rates, (b) selectivity between *p*-GaN and AlGaIn and self-bias voltage on bias power.

To sum up, the final optimized process conditions were determined as  $\text{SF}_6$  concentration of 15%, chamber pressure of 40 mTorr, ICP power of 600 W and bias power of 20 W. Table 1 summarizes the results achieved in our work together with other research using the  $\text{BCl}_3/\text{SF}_6$  mixture. The selectivity in this study is the highest value ever reported, which can be attributed to our systematic optimization and the lowest bias power of our designed etch tool. Additionally, as reported in reference [20], a high selectivity of 33:1 was realized by using a higher frequency bias generator of 40 MHz. The much higher plasma frequency produces lower-energy ions which tends to achieve higher selectivity but with much lower etch rate. This makes the developed process in this work more practical in real device fabrication.

**Table 1.** Comparison of etch conditions, etch rates and selectivity among  $\text{BCl}_3/\text{SF}_6$  mixture selective etching recipes.

Reference	[15]	[21]	This Work	[20]
Generator (MHz)	13.56	13.56	13.56	40
$\text{SF}_6\%$	20	40	15	40
Pressure (mTorr)	37.5	20	40	10
ICP power (W)	200	200	600	/
Bias power (W)	30	60	20	/
GaN etch rate (nm/min)	12	12	3.4	0.529
AlGaN etch rate (nm/min)	0.52	1.3	0.08	0.016
Max. selectivity	23:1	9:1	41:1	33:1

### 3.2. Etched Surface and Plasma Damage Analysis

To comprehensively study the practical effects of the developed process on  $p\text{-GaN}/\text{AlGaN}$  wafer, firstly the etch depth was measured at different etch times by AFM. As seen in Figure 5, the etch process was quite linear until it reached the AlGaN surface. The X-SEM in the inset clearly shows a very smooth and almost non-recessed AlGaN surface after 2.5 min of overetching under the optimized process, demonstrating a highly selective etch to the AlGaN layer.

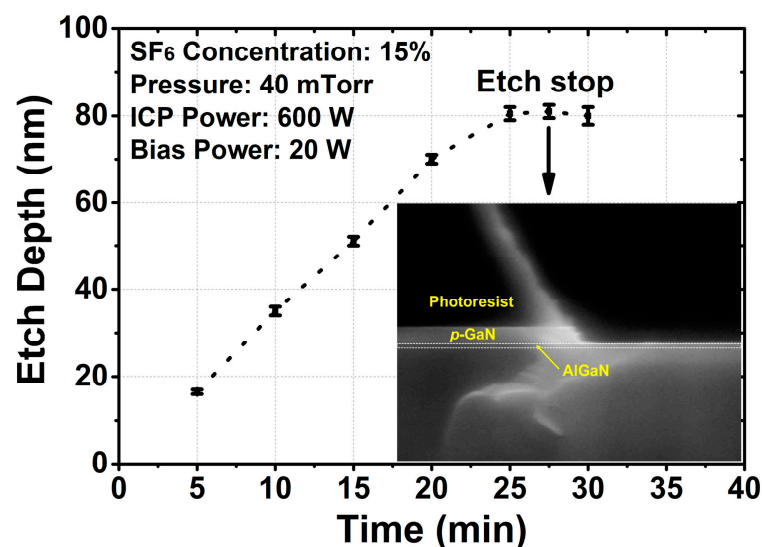


**Figure 5.**  $p\text{-GaN}$  etch depth as a function of time; the inset X-SEM image of sample with 2.5 min of overetching.



To further evaluate the impact of the developed selective etching process on the AlGaIn surface, AFM images ( $5\ \mu\text{m} \times 5\ \mu\text{m}$ ) of the surface morphology were taken in no-contact mode (NCM) for the abovementioned sample (sample A, 2.5 min over etching under the optimized process) and another etched sample by using the nonselective  $\text{BCl}_3/\text{Ar}$  process (sample B) to etch the 80 nm  $p\text{-GaIn}$  layer. The nonselective process has a  $p\text{-GaIn}$  etch rate of approximately 10 nm/min.

As seen in Figure 6, for sample A the exposed AlGaIn surface is quite smooth with the root mean square (RMS) surface roughness of 0.428 nm, which is similar to the as-grown AlGaIn surface (0.446 nm in Figure 6a). This is attributed to the advantage of the developed highly selective etching and its low power causing very minimum surface damage. However, with nonselective  $p\text{-GaIn}$  etching for sample B, the exposed AlGaIn surface roughness reached as high as 0.987 nm. This is equivalent to the as-grown  $p\text{-GaIn}$  surface, which has 1.053 nm RMS roughness due to the doping of  $\text{Cp}_2\text{Mg}$ . Obviously, the sample B AlGaIn surface is much rougher as the morphology is basically inherited from the as-grown  $p\text{-GaIn}$  layer due to the nature of nonselective etching, as illustrated in Figure 6e.

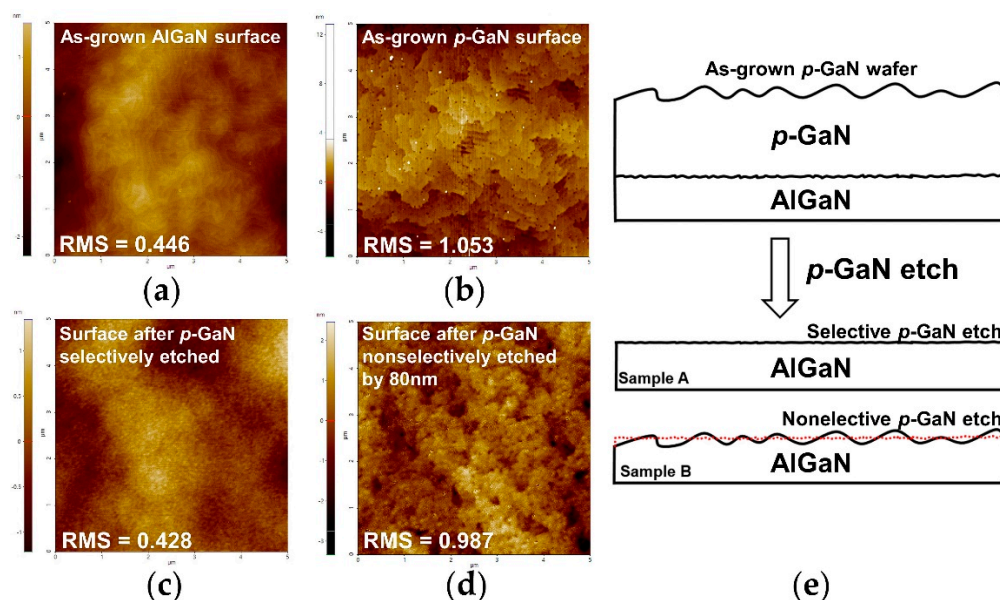


**Figure 6.** Surface morphology of (a) as-grown AlGaIn surface, (b) as-grown  $p\text{-GaIn}$  surface, (c) sample A ( $p\text{-GaIn}$  selectively etched) and (d) sample B ( $p\text{-GaIn}$  nonselectively etched), (e) diagram to illustrate surface morphology for samples A and B.

MIS capacitors were fabricated to evaluate the possible etch damage on the exposed AlGaIn surface for samples A and B. Reference device on as-grown AlGaIn wafer was also prepared for comparison. For all the samples, dilute HCl dip was performed to treat the AlGaIn surfaces, and 25-nm-thick  $\text{Al}_2\text{O}_3$  was deposited at  $300\ ^\circ\text{C}$  using trimethylaluminum (TMA) and  $\text{H}_2\text{O}$  as precursors. Ni/Au bilayers were used as electrodes in the inner circle and exterior zone with a ring gap of  $50\ \mu\text{m}$ . To avoid the possible repair effect on the etch damage, no anneal was performed in this process.

C–V characterizations using a Keithley 4200A are presented in Figure 7. At a quite negative voltage, the capacitance is close to zero because the 2DEG is depleted for all samples. The nearly flat capacitance  $C_{2\text{DEG}}$  indicates that 2DEG has been formed at the AlGaIn/GaN heterojunction interface. For sample A with selective  $p\text{-GaIn}$  etching, the slope of the C–V curve is quite steep and close to the reference as-grown AlGaIn sample, confirming very minimum etch damage on the AlGaIn surface after selective  $p\text{-GaIn}$  removal. However, the slope of the C–V curve for sample B shows an obvious stretch-out, indicating that the exposed AlGaIn barrier layer was degraded during the

nonselective etching of *p*-GaN and thus 2DEG at AlGaN/GaN interface could not be formed efficiently with the gate bias.

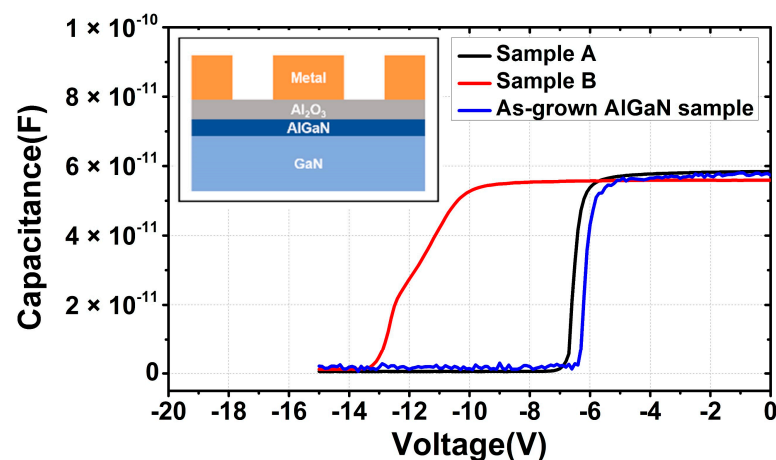


**Figure 7.** C–V characteristics of Ni/Al<sub>2</sub>O<sub>3</sub>/AlGaN MIS capacitors with selective and nonselective *p*-GaN etching. Additionally, as-grown AlGaN sample is referenced here.

#### 4. Conclusions

In this work, a highly selective ICP etch process of *p*-GaN over AlGaN using the BCl<sub>3</sub>/SF<sub>6</sub> mixture was successfully developed, achieving a high selectivity of 41:1. Under the conditions of the optimized SF<sub>6</sub> concentration and chamber pressure, as well as high ICP power, and as low as possible bias power benefiting from our dedicated etch tool, a very smooth and high-quality AlGaN surface could be obtained after *p*-GaN etch. On such AlGaN surface, the fabricated Ni/Al<sub>2</sub>O<sub>3</sub>/AlGaN MIS capacitor showed comparable C–V characteristics to that on the as-epitaxial AlGaN surface. This phenomenon strongly indicated that there was almost no damage on the AlGaN surface after etching the *p*-GaN layer, making this process very promising to be applied on the fabrication of high-performance *p*-GaN gate HEMTs.

**Author Contributions:** Conceptualization, P.Z. and L.W.; methodology, P.Z. and L.W.; validation, K.Z. and M.P.; formal analysis, L.W. and K.Z.; investigation, P.Z. and L.W.; resources, S.X. and C.W. (Chunlei Wu); data curation, P.Z. and L.W.; writing—original draft preparation, P.Z.; writing—review and editing, M.X. and C.W. (Chen Wang); visualization, Y.Y. and R.F.; supervision, M.X., C.W. (Chen Wang) and D.W.Z.; project administration, M.X. and C.W. (Chen Wang); funding acquisition, M.X., C.W. (Chen Wang) and D.W.Z. All authors have read and agreed to the published version of the manuscript.

**Funding:** This research was funded by the National Natural Science Foundation of China, grant number 11904043.

**Data Availability Statement:** Not applicable.

**Conflicts of Interest:** The authors declare no conflict of interest.

#### References

1. Ishida, M.; Ueda, T.; Tanaka, T.; Ueda, D. GaN on Si Technologies for Power Switching Devices. *IEEE Trans. Electron Devices* **2013**, *60*, 3053–3059. [[CrossRef](#)]
2. Marcon, D.; Saripalli, Y.N.; Decoutere, S. 200mm GaN-on-Si epitaxy and e-mode device technology. In Proceedings of the Electron Devices Meeting, Washington, DC, USA, 5–9 December 2015. [[CrossRef](#)]
3. Sacconi, F.; Carlo, A.D.; Lugli, P.; Morkoc, H. Spontaneous and piezoelectric polarization effects on the output characteristics of AlGaN/GaN heterojunction modulation doped FETs. *IEEE Trans. Electron Devices* **2001**, *48*, 450–457. [[CrossRef](#)]
4. Chen, K.J.; Zhou, C. Enhancement-mode AlGaN/GaN HEMT and MIS-HEMT technology. *Phys. Status Solidi* **2011**, *208*, 434–438. [[CrossRef](#)]
5. Scott, M.J.; Fu, L.; Zhang, X.; Li, J.; Yao, C.; Sievers, M.; Wang, J. Merits of gallium nitride based power conversion. *Semicond. Sci. Technol.* **2013**, *28*, 74013. [[CrossRef](#)]

6. Cai, Y.; Zhou, Y.; Chen, K.J.; Lau, K.M. High-performance enhancement-mode AlGaIn/GaN HEMTs using fluoride-based plasma treatment. *IEEE Electron Device Lett.* **2005**, *26*, 435–437. [\[CrossRef\]](#)
7. Saito, W.; Takada, Y.; Kuraguchi, M.; Tsuda, K.; Omura, I. Recessed-gate structure approach toward normally off high-Voltage AlGaIn/GaN HEMT for power electronics applications. *IEEE Trans. Electron Devices* **2006**, *53*, 356–362. [\[CrossRef\]](#)
8. Uemoto, Y.; Hikita, M.; Ueno, H.; Matsuo, H.; Ishida, H.; Yanagihara, M.; Ueda, T.; Tanaka, T.; Ueda, D. Gate Injection Transistor (GIT)—A Normally-Off AlGaIn/GaN Power Transistor Using Conductivity Modulation. *IEEE Trans. Electron Devices* **2007**, *54*, 3393–3399. [\[CrossRef\]](#)
9. Chen, K.J.; Haberen, O.; Lidow, A.; Tsai, C.I.; Ueda, T.; Uemoto, Y.; Wu, Y. GaN-on-Si Power Technology: Devices and Applications. *IEEE Trans. Electron Devices* **2017**, *64*, 779–795. [\[CrossRef\]](#)
10. Roccaforte, F.; Greco, G.; Fiorenza, P.; Iucolano, F. An Overview of Normally-Off GaN-Based High Electron Mobility Transistors. *Materials* **2019**, *12*, 1599. [\[CrossRef\]](#) [\[PubMed\]](#)
11. Marcon, D.; Hove, M.V.; Jaeger, B.D.; Posthuma, N.; Wellekens, D.; You, S.; Kang, X.; Wu, T.-L.; Willems, M.; Stoffels, S.; et al. Direct Comparison of GaN-Based E-Mode Architectures (Recessed MISHEMT and p-GaN HEMTs) Processed on 200mm GaN-on-Si with Au-Free Technology. In Proceedings of the SPIE-The International Society for Optical Engineering, San Francisco, CA, USA, 13 March 2015. [\[CrossRef\]](#)
12. Lukens, G.; Hahn, H.; Kalisch, H.; Vescan, A. Self-Aligned Process for Selectively Etched p-GaN-Gated AlGaIn/GaN-on-Si HFETs. *IEEE Trans. Electron Devices* **2018**, *65*, 3732–3738. [\[CrossRef\]](#)
13. Su, L.-Y.; Lee, F.; Huang, J.J. Enhancement-Mode GaN-Based High-Electron Mobility Transistors on the Si Substrate With a P-Type GaN Cap Layer. *IEEE Trans. Electron Devices* **2014**, *61*, 460–465. [\[CrossRef\]](#)
14. Greco, G.; Iucolano, F.; Roccaforte, F. Review of technology for normally-off HEMTs with p-GaN gate. *Mater. Sci. Semicond. Process.* **2018**, *78*, 96–106. [\[CrossRef\]](#)
15. Buttari, D.; Chini, A.; Chakraborty, A.; McCarthy, L.; Xing, H.; Palacios, T.; Shen, L.; Keller, S.; Mishra, U.K. Selective dry etching of GaN over AlGaIn in BCl<sub>3</sub>/SF<sub>6</sub> mixtures. In Proceedings of the IEEE Lester Eastman Conference on High Performance Devices, Troy, NY, USA, 4–6 August 2004. [\[CrossRef\]](#)
16. Buttari, D.; Chini, A.; Palacios, T.; Coffie, R.; Shen, L.; Xing, H.; Heikman, S.; McCarthy, L.; Chakraborty, A.; Keller, S.; et al. Origin of etch delay time in Cl<sub>2</sub> dry etching of AlGaIn/GaN structures. *Appl. Phys. Lett.* **2003**, *83*, 4779–4781. [\[CrossRef\]](#)
17. Lee, Y.S.; Sia, J.F.; Nordheden, K.J. Mass spectrometric characterization of BCl<sub>3</sub>/SF<sub>6</sub> plasmas. *J. Appl. Phys.* **2000**, *88*, 4507–4509. [\[CrossRef\]](#)
18. Oh, C.S.; Kim, T.H.; Lim, K.Y.; Yang, J.W. GaN etch enhancement in inductively coupled BCl<sub>3</sub> plasma with the addition of N<sub>2</sub> and SF<sub>6</sub> gas. *Semicond. Sci. Technol.* **2004**, *19*, 172–175. [\[CrossRef\]](#)
19. Feng, M.S.; Guo, J.D.; Lu, Y.M.; Chang, E.Y. Materials Chemistry and Physics. Reactive ion etching of GaN with BCl<sub>3</sub>/SF<sub>6</sub> plasmas. *Mater. Chem. Phys.* **1996**, *45*, 80–83. [\[CrossRef\]](#)
20. Beheshti, M.; Westerman, R. Smooth, low rate, selective GaN/AlGaIn etch. *AIP Adv.* **2021**, *11*, 25237. [\[CrossRef\]](#)
21. Qian, R.; Cheng, X.; Zheng, L.; Shen, L.; Zhang, D.; Gu, Z.; Yu, Y. Inductively Coupled Plasma Etching of p-GaN Using Different Masks and Etching Gases. *Semicond. Technol.* **2018**, *43*, 449–455. [\[CrossRef\]](#)